Received: 11 December 2023 | Revised: 19 April 2024 | Accepted: 25 April 2024

DOI: 10.1002/hbm.26706

RESEARCH ARTICLE

WILEY

Microscopic fractional anisotropy outperforms multiple sclerosis lesion assessment and clinical outcome associations over standard fractional anisotropy tensor

F. Vivó[1] | E. Solana[1] | A. Calvi[1] | E. Lopez-Soley[1] | L. B. Reid[2,3] | S. Pascual-Diaz[4] | C. Garrido[5] | L. Planas-Tardido[1] | J. M. Cabrera-Maqueda[1] | S. Alba-Arbalat[1] | M. Sepulveda[1] | Y. Blanco[1] | B. Kanber[6,7] | F. Prados[6,7,8] | A. Saiz[1] | S. Llufriu[1] | E. Martinez-Heras[1]

[1]Neuroimmunology and Multiple Sclerosis Unit Laboratory of Advanced Imaging in Neuroimmunological Diseases (ImaginEM), Hospital Clinic Barcelona, Fundació de Recerca Clínic Barcelona-Institut d'Investigacions Biomèdiques August Pi i Sunyer and Universitat de Barcelona, Barcelona, Spain

[2]Department of Psychiatry, University of California San Francisco, San Francisco, California, USA

[3]Department of Radiology, University of California San Francisco, San Francisco, California, USA

[4]Institute of Neurosciences, Department of Medicine, School of Medicine and Health Sciences, University of Barcelona, Barcelona, Spain

[5]Magnetic Resonance Imaging Core Facility, Institut d'Investigacions Biomèdiques August Pi i Sunyer (IDIBAPS), Barcelona, Spain

[6]Queen Square MS Centre, Department of Neuroinflammation, UCL Queen Square Institute of Neurology, Faculty of Brain Science, University College of London, London, UK

[7]Centre for Medical Image Computing (CMIC), Department of Medical Physics and Bioengineering, University College London, London, UK

[8]E-Health Center, Universitat Oberta de Catalunya, Barcelona, Spain

Correspondence
S. Llufriu and E. Martinez-Heras, Hospital Clinic Barcelona, Calle Villarroel 170, 08036 Barcelona, Spain.
Email: sllufriu@clinic.cat and emartind@recerca.clinic.cat

Funding information
Instituto Carlos III (ISCIII); Plan Estatal de Investigación Científica y Técnica y de Innovación, Grant/Award Numbers: PI15/00587, PI18/01030, PI21/01189; Red Española de Esclerosis Múltiple, Grant/Award Numbers: RD16/0015/0002, RD16/0015/0003; Fundación Merck Salud; Esclerosis Múltiple España (EME)-Red Española de EM (REEM), Grant/Award Number: 2023

Abstract

We aimed to compare the ability of diffusion tensor imaging and multi-compartment spherical mean technique to detect focal tissue damage and in distinguishing between different connectivity patterns associated with varying clinical outcomes in multiple sclerosis (MS). Seventy-six people diagnosed with MS were scanned using a SIEMENS Prisma Fit 3T magnetic resonance imaging (MRI), employing both conventional (T1w and fluid-attenuated inversion recovery) and advanced diffusion MRI sequences from which fractional anisotropy (FA) and microscopic FA (μFA) maps were generated. Using automated fiber quantification (AFQ), we assessed diffusion profiles across multiple white matter (WM) pathways to measure the sensitivity of anisotropy diffusion metrics in detecting localized tissue damage. In parallel, we analyzed structural brain connectivity in a specific patient cohort to fully grasp its relationships with cognitive and physical clinical outcomes. This evaluation comprehensively considered different patient categories, including cognitively preserved (CP), mild cognitive deficits (MCD), and cognitively impaired (CI) for cognitive assessment, as well as groups distinguished by physical impact: those with mild disability (Expanded Disability Status Scale [EDSS]

<=3) and those with moderate–severe disability (EDSS >3). In our initial objective, we employed Ridge regression to forecast the presence of focal MS lesions, comparing the performance of μFA and FA. μFA exhibited a stronger association with tissue damage and a higher predictive precision for focal MS lesions across the tracts, achieving an *R*-squared value of .57, significantly outperforming the *R*-squared value of .24 for FA (*p*-value <.001). In structural connectivity, μFA exhibited more pronounced differences than FA in response to alteration in both cognitive and physical clinical scores in terms of effect size and number of connections. Regarding cognitive groups, FA differences between CP and MCD groups were limited to 0.5% of connections, mainly around the thalamus, while μFA revealed changes in 2.5% of connections. In the CP and CI group comparison, which have noticeable cognitive differences, the disparity was 5.6% for FA values and 32.5% for μFA. Similarly, μFA outperformed FA in detecting WM changes between the MCD and CI groups, with 5% versus 0.3% of connections, respectively. When analyzing structural connectivity between physical disability groups, μFA still demonstrated superior performance over FA, disclosing a 2.1% difference in connectivity between regions closely associated with physical disability in MS. In contrast, FA spotted a few regions, comprising only 0.6% of total connections. In summary, μFA emerged as a more effective tool than FA in predicting MS lesions and identifying structural changes across patients with different degrees of cognitive and global disability, offering deeper insights into the complexities of MS-related impairments.

KEYWORDS
automated fiber quantification, cognitive outcome, diffusion tensor imaging, extended disability status scale, microscopic fractional anisotropy, multiple sclerosis, structural brain connectivity

1 | INTRODUCTION

Multiple sclerosis (MS) is a chronic, demyelinating and neurodegenerative disease of the central nervous system that predominantly affects young adults. It is characterized in its early stages by episodes of neurological dysfunction, which can result in a wide range of physical and cognitive impairments (Estrada-López et al., 2020; Sumowski et al., 2018). Moreover, the clinical manifestations of MS can vary significantly among patients, with some experiencing episodes of symptoms followed by periods of recovery (relapsing–remitting pattern). In contrast, others show a continuous decline in function without distinct periods of remission (progressive form), making diagnosis and management more challenging (Lublin et al., 2014). Conventional magnetic resonance imaging (MRI) plays a critical role in the early diagnosis and monitoring of MS due to its ability to detect the presence of characteristic white matter (WM) lesions and track longitudinal changes in lesion load (Lassmann et al., 2007; Thompson et al., 2018). However, conventional MRI primarily focuses on the macroscopic features of the disease and has a limited capacity to inform on the underlying microscopic tissue alterations and various phenotypic properties of MS (Bakshi et al., 2008).

Diffusion MRI (dMRI) is an advanced imaging modality that enables non-invasive, in vivo characterization of microscopic cellular arrangements by measuring the random translational motion of water molecules. Standard diffusion tensor imaging (DTI) (Basser & Pierpaoli, 1996) has been widely used in clinical practice and neuroimaging research due to its simplicity and sensitivity to WM tissue changes, enabling brain connectivity mapping (Reid et al., 2017). For example, computing the mean fractional anisotropy (FA) of streamlines delineated with tractography is a traditional approach of assessing structural connectivity (Llufriu et al., 2017; Martinez-Heras et al., 2023). However, earlier publications have highlighted the limitations of DTI in representing complex fiber patterns within a voxel (Landman et al., 2010; Wiegell et al., 2000). Advanced biophysical multi-compartment diffusion models, such as the multi-compartment spherical mean technique (MC-SMT), which rely on more complex diffusion encoding sequences, have been developed to overcome the limitations of conventional diffusion tensor approaches (Kaden et al., 2016). These techniques have been shown to successfully decompose underlying crossing-fiber patterns, providing more accurate fiber reconstruction and a deeper understanding of WM microstructure (Martinez-Heras et al., 2021). One such MC-SMT derived metric is microscopic FA (μFA), which offers a refined depiction of anisotropic diffusion, particularly within the intra-axonal structure, enhancing our understanding of microstructural complexities in MS (Bagnato et al., 2019).

Although MS global lesion load demonstrates a weak correlation with physical and cognitive disease progression, lesion localization

and typology are promising biomarkers for disability related to the disease (Calvi et al., 2022). Advanced dMRI methods are highly effective for assessing lesion damage, owing to their capacity for detecting subtle microstructural alterations, including neurodegenerative tissue damage (Martínez-Heras et al., 2020). In structural connectivity studies, a frequently used approach is to gather an average diffusion metric over each tract, a method that might overlook critical information about the specific locations and extent of tissue damage. In contrast, a detailed analysis of diffusion measures along WM bundles can yield a more accurate representation of tissue characteristics, potentially offering greater insights into how these diffusion measures change in the presence of brain damage (Sbardella et al., 2013). Given this context, we sought to assess the capabilities of FA and μFA in identifying focal tissue damage and associating these findings with clinical outcomes in MS. We included FA in our analysis as an acknowledgement as to its prominence in connectivity analyses, and compared these results with those of with μFA. Taking into account the limitations of DTI in depicting complex fiber structures and the benefits of multi-compartment models, we hypothesized that μFA is not only a more sensitive metric for quantifying both focal and diffuse MS damage compared to standard FA, but also successfully identify hidden patterns that FA fails to recognize in structural brain connectivity regarding clinical outcome analysis for both cognitive and physical evaluations.

2 | METHODS

2.1 | Participants

A sample of 76 people with MS (PwMS) was prospectively recruited at the MS unit of the Hospital Clinic of Barcelona, with the following inclusion criteria: diagnosis of MS according to the 2017 McDonald criteria (Thompson et al., 2018). Only PwMS with either a relapsing–remitting or secondary progressive MS were included. The Ethics Committee at the Hospital Clinic of Barcelona approved the study, and all participants gave informed written consent for research and publication.

2.2 | Cognitive and physical evaluations

Cross-sectional comprehensive demographic data—including age, gender, educational tenure, and socioeconomic indicators—were obtained for each participant during their respective study visits. Clinical evaluations primarily revolved around two key dimensions: the assessment of attention and processing speed, and the evaluation of global disability. The former was assessed using the Symbol Digit Modalities Test (SDMT) (Parmenter et al., 2007), while the latter was measured with the Expanded Disability Status Scale (EDSS), as suggested by Kurtzke (Kurtzke, 1983). Cognitive abilities of PwMS were indexed using z-scores from the SDMT (zSDMT) (Strober et al., 2020), adjusted for age, gender, and educational background. For a deeper, more nuanced connectivity analysis, we dissected the collective sample, aiming to unravel the cognitive impact of the disease in segmented groups. Patients were stratified based on their zSDMT values into distinct categories: cognitively impaired (CI; zSDMT <-1.5), mild cognitive deficits (MCD; zSDMT from -0.5 to -1.5, both included), and cognitively preserved (CP; zSDMT >-0.5). PwMS were also categorized into two groups based on their EDSS scores: those with scores below 3.0 were considered physically mildly affected PwMS while those with scores of 3.0 or higher were considered to have a moderate–severe physical disability (Coll et al., 2023).

2.3 | MRI: Acquisition and processing

2.3.1 | Structural and diffusion magnetic resonance acquisition

MR sequences were acquired on a SIEMENS Magnetom Prisma 3T scanner with a 64-channel phased-array head/neck coil. Structural sequences included 3D-Magnetization Prepared Rapid Acquisition Gradient Echo (MPRAGE), and 3D T2 fluid-attenuated inversion recovery (FLAIR) sequences. The 3D MPRAGE sequence parameters were: TR = 1800 ms; TE = 3.01 ms; TI = 900 ms; 240 sagittal slices with 0.94 mm isotropic voxel size and a 256 × 256 matrix size. The 3D T2 FLAIR sequence parameters were: TR = 5000 ms; TE = 379 ms; TI = 1800 ms; 208 sagittal slices with 0.94 mm isotropic voxel size and a 256 × 256 matrix size. Diffusion MRI sequences were acquired utilizing a multi-shell approach, encompassing two distinct phase encoding directions: posterior–anterior and anterior–posterior, each with 90 volumes, summing up to a total of 180 volumes. The acquisition parameters were as follows: TR = 5400 ms; TE = 113 ms; parallel acceleration factor = 4; phase partial Fourier = 6/8; 100 contiguous axial slices at 1.5 mm isotropic voxel dimension with no gap; a 150 × 150 matrix size. The b-values were acquired in an interspersed pattern: 30 directions at 1000 s/mm^2, 60 directions at 2000 s/mm^2, 90 directions at 3000 s/mm^2, and $5 \times b = 0$ volumes. The total acquisition time was 8:50 minutes for each phase encoding direction.

2.3.2 | MS lesion segmentation

MS lesions were manually delineated on the T1 3D MPRAGE image, supported by a co-registered FLAIR image, using a semiautomated edge finding tool (Jim version 6.0 Xinapse System, http://www.xinapse.com/). We omitted lesions smaller than 27 mm^3 because they fall below the diagnostic size threshold for typical MS lesions (Filippi et al., 2019).

2.3.3 | dMRI processing

We employed an extensive dMRI preprocessing strategy, encompassing MP-PCA denoising, Gibbs ringing removal, eddy current and

motion correction, geometric unwarping, and bias field correction using FSL and MRtrix software packages (Tournier et al., 2019). FA was calculated using all $b = 1000$ s/mm^2 volumes via the weighted least squares fitting method implemented in FSL (Basser et al., 1994). We also fitted the microscopic diffusion tensor using all diffusion b-shells through MC-SMT software (https://github.com/ekaden/smt) (Kaden et al., 2016). We then applied an inverse transformation matrix via boundary-based registration to integrate MS lesions into the dMRI's space using epi_reg in FSL, effectively transforming the lesion masks from the MPRAGE space to the dMRI space (Greve & Fischl, 2009).

2.3.4 | Automated fiber quantification analysis

To evaluate the sensitivity of anisotropy diffusion metrics for quantifying both focal and diffuse MS damage, we used the automated fiber quantification (AFQ) open-source library (https://github.com/yeatmanlab/pyAFQ) implemented in Python to generate tract diffusion profiles for each target WM bundle (Yeatman et al., 2012). To segment the WM fiber tracts, we employed a semiautomatic method using the TractSeg tool (https://github.com/MIC-DKFZ/TractSeg) (Wasserthal et al., 2018). This method was applied to evaluate specific bilateral bundles of interest, including the optic radiation, corticospinal, arcuate fasciculus, and corpus callosum. These long bundles were selected due to their connection to WM regions commonly affected by the neuropathological burden in MS and their involvement in its clinical manifestations (Lipp et al., 2020; Llufriu et al., 2012; Meijer et al., 2020). This fast and accurate segmentation process, which did not require the use of tractography, was based on data collected from 105 subjects selected from the Human Connectome Project. In order to mitigate the impacts of MS lesions on the accuracy of tract reconstruction pathways within the AFQ framework, we incorporated both the lesion mask and the normal-appearing WM tissue into the peaks of the fiber orientation distribution function (Solana et al., 2018). Then, the AFQ algorithm performed iterative comparisons between reconstructed fibers, deriving a mean tract trajectory based on their distances and lengths. This process involves several key steps, including resampling each streamline into 100 equidistant segments and calculating the fiber tract core as the average of each x, y, and z coordinate. Subsequently, the spread of fibers is determined by computing the covariance between nodes. The algorithm then refines the core representation by iteratively calculating the Mahalanobis distance for each fiber node and removing outlier fibers that significantly deviate from the core or mean fiber length (Yeatman et al., 2012). This iterative procedure continues until a stable core representation is obtained.

Once the mean tract trajectory is established, the resulting 100 equidistant segments can be interpolated with values for each diffusion-derived parameter (FA and μFA) across all nodes along the targeted WM bundle streamlines (Bain et al., 2019). Figure 1 summarizes the processing pipeline; since the whole brain tractography computation (Figure 1a), through bundle extraction and AFQ implementation to divide WM bundles into 100 segments (Figure 1b,c), to finally extract the diffusion tract profile measures of those bundles (Figure 1d).

2.3.5 | Structural connectivity analysis

To evaluate how sensitive FA and μFA were in a brain connectivity analysis with respect to detecting clinical outcomes, we started by computing fiber orientation distributions through constrained-spherical deconvolution (Jeurissen et al., 2014). Subsequently, we executed a whole-brain probabilistic tractography using the iFOD2 algorithm, with the WM (encompassing both the normal-appearing WM and the lesion mask) as the seeding region. This process generated 6 million streamlines, guided by the five-tissue-type model and anatomical exclusion criteria (Martínez-Heras et al., 2015; Smith et al., 2012). Simultaneously, lesion-filled T1-weighted images were segmented into 62 cortical regions according to the anatomical Desikan-Killany atlas using the Mindboggle software package (Klein et al., 2017). Additionally, 14 deep gray matter (dGM) regions were delineated through the FSL-FIRST pipeline (Patenaude et al., 2011).

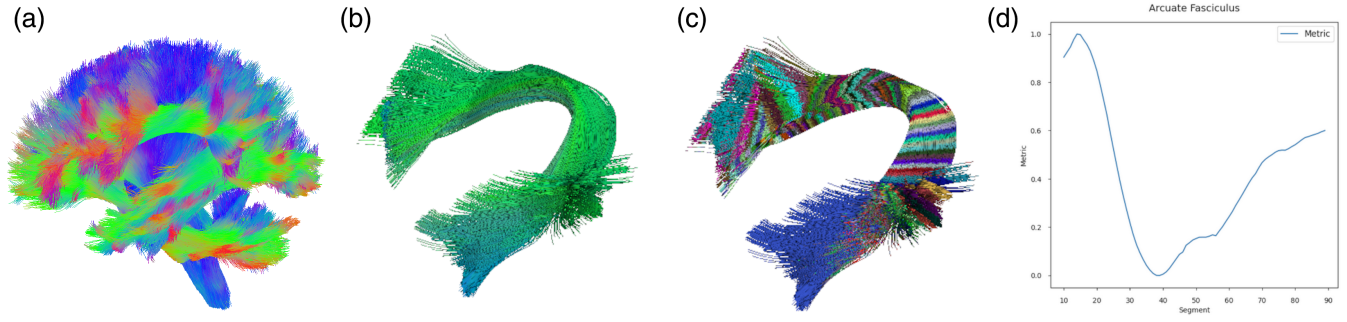

FIGURE 1 Automated fiber quantification (AFQ) processing pipeline. (a) Whole brain tractography from the Human Brain Connectome project atlas, (b) arcuate fasciculus tract extracted from the whole brain tractography, and (c) division of the arcuate fasciculus tract into 100 segments using the AFQ methodology. (d) Tract profile delineation of the arcuate fasciculus bundle using fractional anisotropy (FA) measures, where the x-axis represents the tract segment and the y-axis represents the diffusion measure.

Then, these 76 segmented brain regions were assigned as the nodes of the network.

To quantify the FA-weighted adjacency matrices from the streamlines tractography, we computed the mean FA and μFA across 2850 WM connections formed between all pairs of cortical and dGM nodes of the network (Llufriu et al., 2017). Following this, any connections not present in at least 85% of the cases were removed to avoid analysis of spurious connections. In the end, 673 connections were preserved. From these connections, missing values are interpreted as false negatives, under the assumption that genuine connectivity exists between the regions in question. However, this connectivity remains undetected, likely due to constraints in sensitivity or the overall quality of the sequence. In line with this assumption and to address these undetected connections, we have employed linear regression techniques for imputation.

2.4 | Statistical analysis

Descriptive statistics were reported as median and interquartile range (IQR: 25th–75th percentiles) for quantitative variables and as absolute frequency and percentage for qualitative variables. Normality assumptions were confirmed through the Shapiro–Wilk test and by visually inspecting the frequency distribution of the variables assessed. Pearson correlation coefficients were calculated to assess the relationships between diffusion anisotropy measurements (FA and μFA) and clinical variables, while standard ordinary least squares regression was employed to examine their association with tissue damage.

The relationship between anisotropy metrics obtained from the AFQ analysis and tissue damage was individually evaluated for each tract using linear regression models. The *R*-squared value was used as the evaluation metric.

For the structural connectivity analysis, age and gender effects were adjusted using linear regression (Solana et al., 2019) before applying the Mann–Whitney *U* test to assess statistical differences in connections between groups of PwMS, controlling for multiple comparisons using the Benjamini–Hochberg Procedure (FDR <0.05). Additionally, the effect size was calculated to quantify the magnitude of these differences using Cohen's *d* formula. In light of our study's sample size, we adopted a conservative analytic approach, prioritizing observations with a substantial effect size (Cohen's *d* >0.8). This decision is rooted in our commitment to highlight findings of potential practical significance while also acknowledging the increased susceptibility of smaller samples to statistical noise, outliers, and both Type I and II errors. Our focus on larger effect sizes offers a balance between robustness of findings and the inherent variability of small-sample research.

In order to assess the performance of the models and enable comparison, we used the *R*-squared metric, and in addition, we implemented residual plots to validate the constructed models. All analyses were performed with a two-tailed Type I error threshold of 5% and a significance level set at $p < .05$.

TABLE 1 Demographic, clinical, and MRI characteristics.

Age, years [IQR]	49.6 [41.1–56.5]
Female, *n* (%)	57 (75)
MS type, *n* (%)	
Relapsing–remitting	63 (83)
Secondary progressive	13 (17)
Disease duration, years [IQR]	16.2 [12.7–21.2]
Expanded Disability Status Scale (EDSS), median (range)	2.0 (1.0–6.5)
z-Score Symbol Digit Modalities Test (zSDMT), median [IQR]	−1 [−0.43 to −1.9]
Normalized lesion volume (cm^3) [IQR]	12.48 [I4.46–25.67]
Normalized brain volume (cm^3) [IQR]	1380 [1311.92–1461.01]

3 | RESULTS

3.1 | Demographic and clinical evaluations

Table 1 presents the demographic and clinical data for the 76 PwMS. The majority were female (75%) with a median age of 49.6 years (IQR 41.1–56.5). Most had relapsing–remitting MS (83%). Patients demonstrated moderate disability, as evidenced by a median EDSS score of 2.0 for clinical evaluation and a median SDMT score of −1 (IQR −0.43 to −1.9) for cognitive evaluation. Four participants underwent solely clinical assessments, without subsequent cognitive monitoring. In the study, subjects were divided into different categories according to the clinical outcomes: 25 in the CI group, 24 in the MCD group, 23 in the CP group for cognitive evaluation, and two additional groups based on physical evaluations, with 50 subjects considered physically mildly affected PwMS (EDSS scores below 3.0) and 26 subjects considered to have a moderate–severe physical disability (EDSS scores of 3.0 or higher).

3.2 | Evaluation of tissue damage

We employed the AFQ methodology for this analysis to study the relationship between anisotropy diffusion metrics and lesion volume inside each assessed tract. This approach allowed for precise quantification of the sensitivity of these metrics in response to focal MS lesions. To statistically validate the differences in model results between μFA and FA, we conducted an ANOVA test. The results indicated a significant difference (*p*-value <.001), with μFA significantly outperformed standard FA in explaining variance in lesion volume in every bundle assessed (Table 2), yielding a mean *R*-squared of .57 compared to FA's 0.24. In most WM tracts examined—including the corticospinal, arcuate fasciculus, and corpus callosum—μFA consistently registered *R*-squared values nearly threefold that of

TABLE 2 Comparative analysis of anisotropy diffusion metrics (FA and μFA) in regarding lesion volume in various white matter tracts using AFQ methodology.

Tract	Hemisphere	Lesion volume (mean, % cm^3)	*R*-squared FA	*R*-squared μFA
Optic radiation	R	11.3	.39	.65
	L	10.5	.38	.65
Corticospinal	R	2.5	.12	.29
	L	2.6	.14	.38
Arcuate fasciculus	R	6.1	.22	.71
	L	5.1	.21	.67
Corpus callosum	-	5.6	.22	.66
Average (SD)			.24 ± .10	.57 ± .15

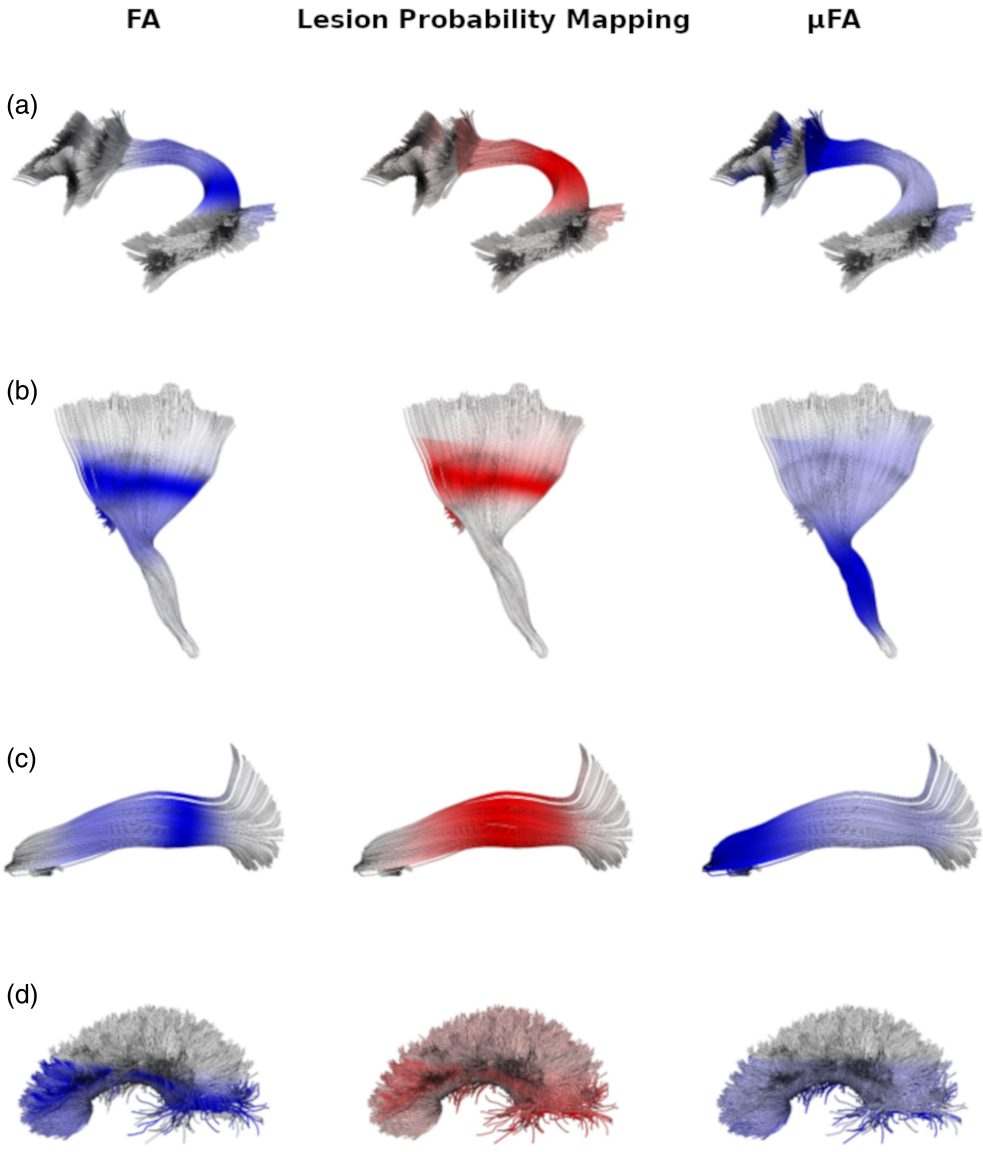

FIGURE 2 The figure illustrates diffusion metrics throughout various segments of white matter (WM) tracts, such as the arcuate fasciculus (a), corticospinal tract (b), optic radiation (c), and corpus callosum (d), with each tract distinctively colored to represent specific diffusion characteristics and the likelihood of lesions. Areas marked in red within the tracts suggest regions with an increased probability of lesions, while the blue and light blue hues indicate the levels of fractional anisotropy (FA) and microscopic fractional anisotropy (μFA) values, respectively.

FA. However, in the case of the optic radiation tract, while μFA still surpassed FA, the margin of superiority was more nuanced.

Following this analysis, Figure 2 illustrates the comparative effectiveness of FA and μFA in representing WM fiber characteristics and their response to focal lesion damage. In this depiction, μFA demonstrates a superior ability to capture the morphology and fundamental diffusion properties of the WM fibers, more accurately correlating with the areas of higher lesion probability, as indicated in red in the

central panel and corresponding with the decreased μFA values in light blue on the right. Conversely, FA, while still indicative of changes in WM fibers, shows a broader, less specific distribution of reduced values, as seen on the left side of the figure.

3.3 | Structural connectivity analysis

In our comparative analysis of PwMS groups based on cognitive performance, μFA appeared to be more sensitive than FA in detecting brain connectivity differences between groups in terms of number of statistically significant connections (Figure 3). When contrasting the CP and MCD groups, from a total of 673 connections, FA detected 4 modifications (0.5%), while μFA revealed 17 (2.5%). FA found limited changes, primarily in the dGM regions—right thalamus with both left putamen and left pallidum and left caudate with right pars orbitalis. In contrast to FA measure, μFA revealed numerous brain connections with significant differences, emphasizing the substantial extent of these changes as quantified by their effect sizes. Notable differences involved connections between the left medial temporal region and dGM sections, and within the left frontal brain region. We also identified decreased WM connectivity within the right cingulate cortex.

Significant cognitive differences between CP and CI groups resulted in numerous statistically significant connections compared to other groupwise comparisons with higher effect sizes, evidenced by FA detecting changes in 38 out of 673 connections (5.6%), while μFA flagged 219 changes (32.5%). Still, despite showing differences between groups, FA displayed a narrower range of affected connections with lower effect sizes compared to μFA. Microstructural FA displayed general interhemispheric differences, mainly impacting regions between dGM and all cortex lobes, specifically the frontal cortex. We also found significant changes in connectivity between the parietal cortex and both the frontal and medial temporal cortices.

When comparing MCD and CI groups, FA only found differences in 2 of the 673 connections: the left putamen with left lingual gyrus, and the right pericalcarine with the right precuneus. By contrast, μFA found 33 affected connections, mainly involving connections between bilateral dGM regions—putamen, thalamus and insula—with frontal cortex regions, highlighting the superior frontal lobe.

In our analysis concerning connectivity within physically affected groups, identifying statistically significant differences in connectivity proved to be more challenging. Nevertheless, μFA was able to detect notable differences in connectivity, particularly between the left dGM and both the left frontal cortex lobe and the left temporal medial lobe (Figure 4). Conversely, FA identified only a handful of significantly different connections, notably between the left putamen and the left occipital cortex.

4 | DISCUSSION

In this study, we directly compared the sensitivity of μFA and FA to local and diffuse tissue damage related to MS, examining their response in two distinct ways: first, by assessing the detection of MS lesion changes, and second, by evaluating their ability to detect changes in brain connectivity related to the degree of cognitive and physical disability.

The analysis based on the AFQ methodology revealed that μFA was a more sensitive and specific metric of focal and diffuse MS damage. The limitations of FA became evident when modeling the relationship between this measure and localized focal tissue damage, where it only achieved a mean *R*-squared of .24. This limitation likely stems from FA's inability to account for intra-voxel variations, leading to a lack of detail in capturing complex tissue structures (Andersen et al., 2020). By contrast, μFA, with its enhanced capability to model crossing fibers more accurately, achieved higher *R*-squared values (mean of .57), making it a more reliable indicator of the disease's severity in terms of lesions damage. Further exploring the limitations identified in FA, it is notable that the optic radiation tract, a region commonly affected by MS (Gabilondo et al., 2014), showed a relatively improved FA performance compared to other tracts. Nonetheless, this performance was substantially lower than that of μFA. Here, FA demonstrated a relatively higher *R*-squared value of .38 in contrast to μFA, which attained a higher *R*-squared value of .68. This FA performance in the optic radiation can be attributed to its anatomy, which has fewer crossing fibers, unlike many tracts commonly impacted by MS. This result aligns with our broader observation that both FA and μFA metrics show improved performance in WM bundles with more pronounced tissue damage. Moreover, the lower percentage of lesion load in tracts like the corticospinal tract makes them more challenging to predict, highlighting the richer data available for tracts with larger lesion volumes and thus facilitating more accurate predictions.

In our comparative analysis of PwMS groups based on cognitive abilities, μFA was more adept than FA in detecting subtle differences in brain connectivity. Specifically, μFA emerged as a more sensitive and robust metric for detecting key connections across various group comparisons. During the comparison of the CP and MCD groups, despite the inherently limited number of altered connections, μFA successfully identified crucial connectivity deficits. This capability of μFA was even more pronounced in the CP and CI group comparison, where it revealed extensive interhemispheric changes, especially in the interactions between dGM structures such as the thalamus, caudate, and putamen with cortical lobes. Significantly, changes were found in regions related to the superior frontal gyrus, vital for attention and decision-making, were noted, indicating potential impacts on cognitive functions in MS patients (Friedman & Robbins, 2021) (Sepulcre et al., 2009). In the comparison between MCD and CI groups, while FA had difficulties in identifying significant differences, μFA successfully recognized alterations, especially in bilateral dGM regions. Noteworthy changes in connections, such as between the left caudal anterior cingulate and the thalamus, and between the superior frontal lobe and dGM regions, were observed. These areas are crucial for cognitive functions like attention and executive processes (Zhang et al., 2021), suggesting that altered connectivity can affect cognitive tasks in MS patients.

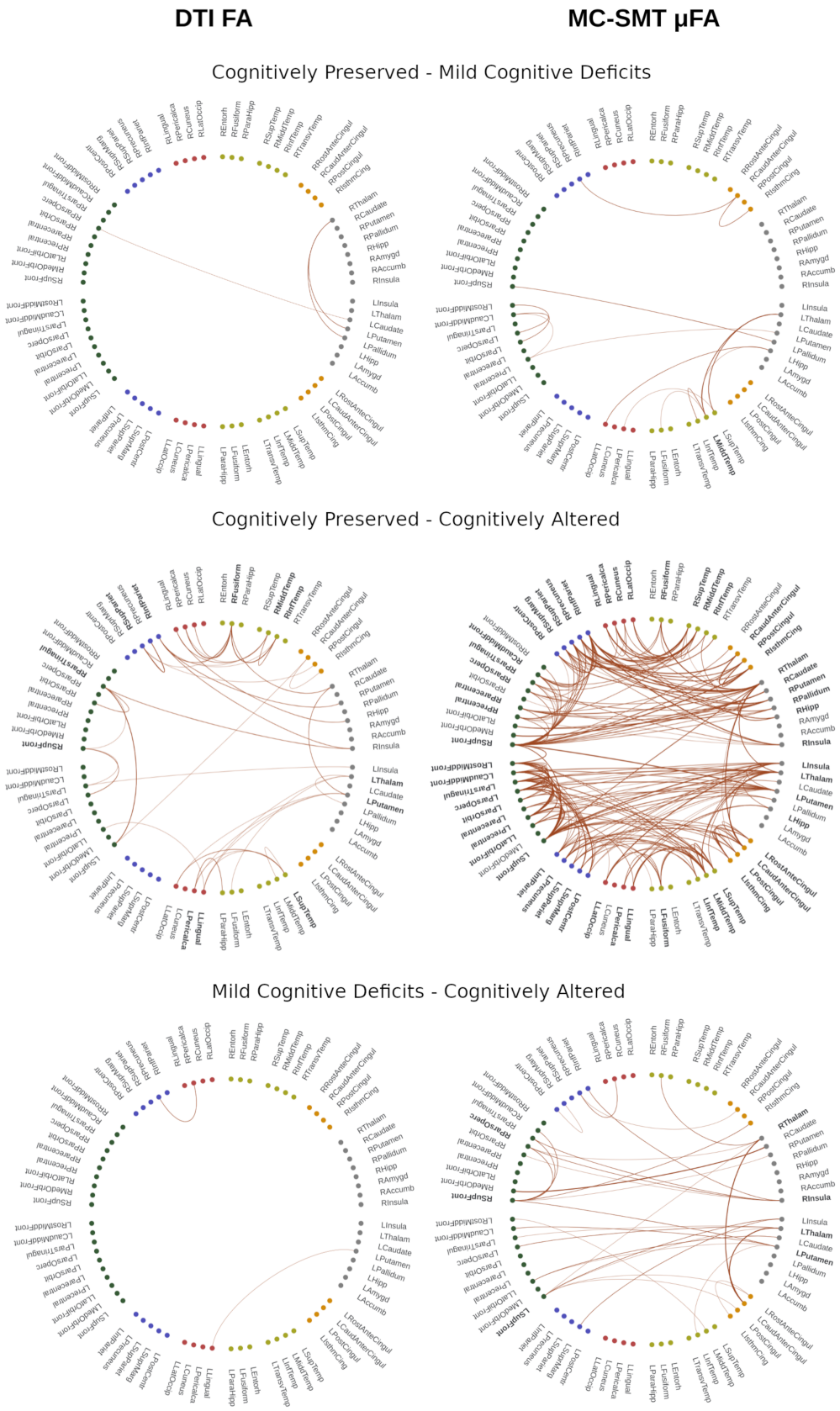

FIGURE 3 Comparative analysis of brain connectivity alterations in people diagnosed with multiple sclerosis (PwMS) groups based on cognitive capabilities using fractional anisotropy (FA) and microscopic FA (μFA). The circular plots (connectograms) display two distinct fitting models of fractional anisotropy: diffusion tensor imaging (DTI) on the left and multi-compartment spherical mean technique (MC-SMT) on the right. Each connectogram contains colored dots, signifying different brain regions of interest. Connecting lines, indicative of significant differences in connections between these regions, are shown with an effect size greater than 0.8. The red color on these lines denotes a decreased value in each diffusion-derived parameter (FA and μFA).

In the context of physically impaired groups, despite the inherent challenges, μFA managed to detect significant connections while FA found few. Microstructural FA modifications in structural connectivity were located between dGM, notably the thalamus, caudate, and putamen, and the frontal areas, particularly the superior frontal cortex. These WM connections are closely related to a fundamental role in

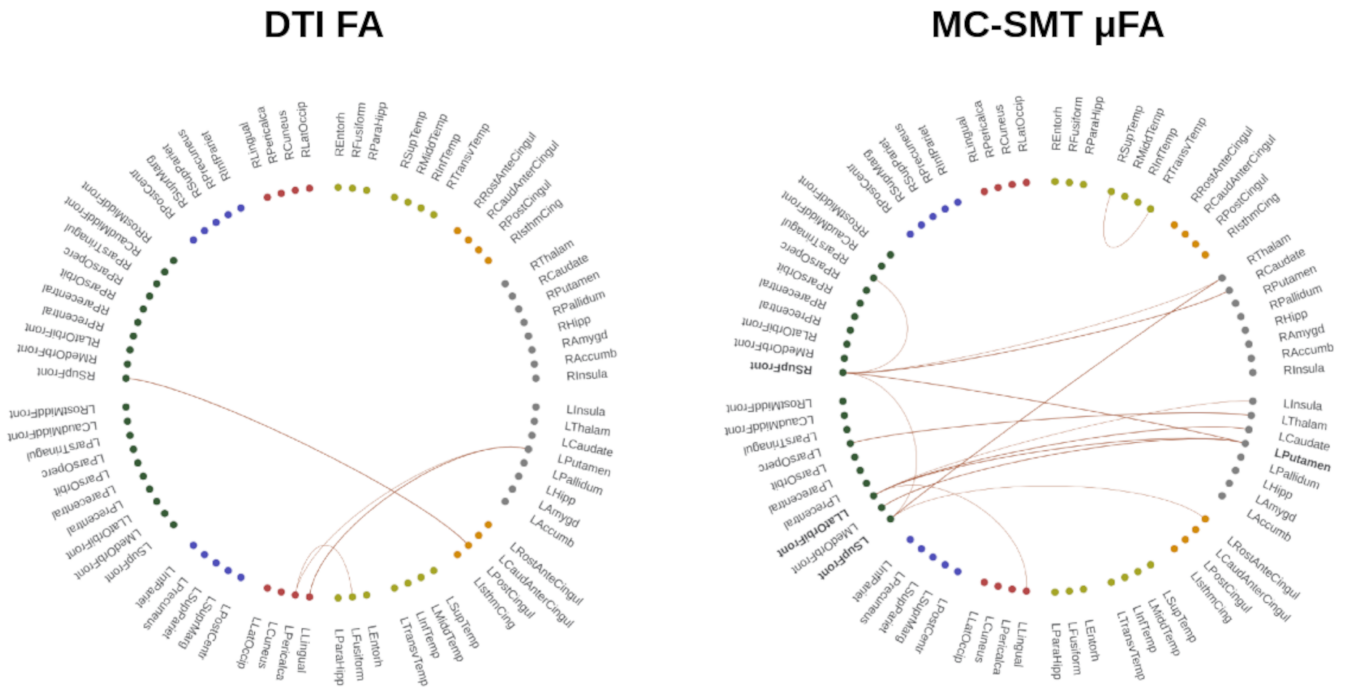

FIGURE 4 Comparative analysis of brain connectivity alterations in two groups of people diagnosed with multiple sclerosis (PwMS) differentiated by physical disability (Expanded Disability Status Scale [EDSS] <3 and ≥EDSS 3), using fractional anisotropy (FA) and microscopic FA (μFA). The circular plots (connectograms) display two distinct fitting models of fractional anisotropy: diffusion tensor imaging (DTI) on the left and multi-compartment spherical mean technique (MC-SMT) on the right. Each connectogram contains colored dots, signifying different brain regions of interest. Connecting lines, indicative of significant connections between these regions, are shown with an effect size greater than 0.8. The red color on these lines denotes a decreased value in each diffusion-derived parameter (FA and μFA)

motor planning and execution, intertwined with cognitive processes. The thalamus, as a relay center, integrates sensory and motor signals, while the caudate and putamen, essential for voluntary motor movements and procedural learning, collaborate with the superior frontal cortex in executive functions and decision-making (Friedman & Robbins, 2021; Shine et al., 2023; Zhang et al., 2021). The observed modifications suggest that these patients may not only experience motor challenges, but also face difficulties in tasks requiring simultaneous cognitive processing and motor coordination.

To sum up, our investigation into the sensitivity of anisotropy diffusion metrics concerning MS lesions underscores the superior capability of μFA over FA in understanding WM tissue damage. While FA provides a generalized view of WM changes, μFA emerges as a more sensitive measure. Importantly, the connections identified by μFA not only outnumbered those detected by FA but also exhibited larger effect sizes, indicating a more significant impact. This enhanced detection capability of μFA offers a clearer understanding of the neurological shifts, especially when assessing changes in line with clinical stratifications like zSDMT and EDSS scores. In contrast to FA, which may overlook more subtle yet clinically relevant differences, μFA's ability to uncover a greater number of connections with notable effect sizes strengthens. Nevertheless, it is essential to acknowledge certain limitations of our study. Firstly, the cross-sectional nature of the study restricts its insights to a single snapshot in time, making it challenging to elucidate the progression or dynamic changes associated with MS. This design does not capture the potential longitudinal variations and developments in patients' brain structures and clinical outcomes. Another possible limitation of the study is the mean EDSS score of 2, reflecting a mild level of disability among participants. This might limit the applicability of findings to populations with more severe MS. Despite this, the demographic data provide a clear snapshot of the disease spectrum. Moreover, while dMRI offers advanced imaging capabilities, it is worth noting that our study did not incorporate the quantification of lesions in the spinal cord, a known contributor to physical disability in MS. Lastly, in this study, our primary emphasis was on comparing FA with μFA, utilizing both the DTI and MC-SMT models. However, numerous other diffusion microstructure imaging techniques are available, each characterized by distinct protocols, underlying assumptions, and methods of signal representation. This includes phenomenological signal representations such as free water elimination and diffusion kurtosis imaging as well as more sophisticated biophysical multi-compartment models like neurite orientation dispersion and density imaging and WM tract integrity (Martinez-Heras et al., 2021). Future research should explore these techniques to provide a more comprehensive understanding of tissue microstructures beyond the MC-SMT model. Finally, building on the findings of our research, it becomes evident that this study holds considerable implications for both clinical practice and medical research. The superior sensitivity and specificity of μFA over

traditional FA positions it as a promising tool in early detection and characterization of neurological changes. μFA provide new insights into the intricate complexities of neurological diseases, setting the stage for more targeted therapeutic research. The accuracy and biological relevance of the connections identified by μFA provide a reliable foundation for ongoing and future neurological studies.

AUTHOR CONTRIBUTIONS

F.V was involved in writing and revising the manuscript, analyzing and interpreting data, and in the design and conceptual framework of the study, including statistical analysis. E.S., A.C., E.L.-S., L.B.R., S.P.-D., C.G., L.P.-T., J.M.C., S.A.-A., M.S., Y.B., B.K., F.P., and A.S. contributed to the manuscript's development and refinement, significantly aiding in the interpretation of findings, and the study's conceptualization. E.M.-H. and S.L.D. were instrumental in drafting and revising the manuscript, played a pivotal role in data acquisition, and participated in the analysis, interpretation, and conceptualization of the research.

ACKNOWLEDGMENTS

The authors are grateful to the MRI core facility of the Institut d'Investigacions Biomèdiques August Pi i Sunyer (IDIBAPS) and to the Fundació Cellex for their support. This work was partially developed at the building Centro Esther Koplowitz, Barcelona, CERCA Programme/Generalitat de Catalunya. This work was sponsored by the Instituto Carlos III (ISCIII) and co-funded by the European Union through the Plan Estatal de Investigación Científica y Técnica y de Innovación 2015–2024 (PI15/00587, PI18/01030, and PI21/01189 to SL and AS and SL); by the Red Española de Esclerosis Múltiple (REEM—RD16/0015/0002, RD16/0015/0003); by Bristol Myers Squibb, the Ayudas Merck de Investigación 2017 from the Fundación Merck Salud and Esclerosis Múltiple España (EME)-Red Española de EM (REEM) 2023 grant. None of the funding bodies had any role in the design or performance of the study; the collection, management, analysis and interpretation of the data; the preparation, revision or approval of the manuscript; or the decision to submit the manuscript for publication.

CONFLICT OF INTEREST STATEMENT

The authors have no competing interests with respect to this research. F.V., L.B.R., S.P.-D., C.G., L.P.-T., S.A.-A., and E.M.-H. have nothing to disclose. E.S. received travel reimbursement from Sanofi, Merck and ECTRIMS; A.C is supported by the ECTRIMS postdoc fellowship (2022), previously received a UK MS Society PhD studentship (2020), a Guarantors of Brain "Entry" clinical fellowship (2019), and an ECTRIMS-MAGNIMS fellowship (2018). He received travel reimbursement from UK MS society, ECTRIMS, NAIMS. B.K and F.P are funded by National Institute for Health Research (NIHR) University College London Hospitals (UCLH) Biomedical Research Centre. FP was funded by a Guarantors of Brain non-clinical Postdoctoral Fellowship. E.L.-S. holds a predoctoral grant from the University of Barcelona (APIF) and she received travel support from Sanofi; M.S. received speaking honoraria from Roche, Biogen, Bial, and Horizon Therapeutics and travel reimbursement from Biogen, Sanofi, Merck, Bial, and Roche for national and international meetings; J.M.-C. received speaker honoraria from Sanfi; A.S. received compensation for consulting services and speaker honoraria from Bayer-Schering, Merck-Serono, Biogen-Idec, Sanofi-Aventis, TEVA, Novartis, and Roche; S.L. received compensation for consulting services and speaker honoraria from Biogen Idec, Novartis, TEVA, Genzyme, Sanofi, Merck, and Bristol-Myers Squibb, and holds grants from the Instituto de Salud Carlos III.

DATA AVAILABILITY STATEMENT

Imaging data in BIDS format and MRI protocol files that support the findings of this research can be obtained upon a reasonable request to the corresponding authors.

ORCID

F. Vivó https://orcid.org/0000-0002-6409-1197
E. Solana https://orcid.org/0000-0001-7973-2439
A. Calvi https://orcid.org/0000-0002-1953-2803
E. Lopez-Soley https://orcid.org/0000-0002-2183-8094
L. B. Reid https://orcid.org/0000-0002-3585-8141
S. Pascual-Diaz https://orcid.org/0000-0001-5871-5867
L. Planas-Tardido https://orcid.org/0009-0002-4060-5824
J. M. Cabrera-Maqueda https://orcid.org/0000-0002-6984-1209
S. Alba-Arbalat https://orcid.org/0000-0003-1662-2317
M. Sepulveda https://orcid.org/0000-0002-3078-645X
Y. Blanco https://orcid.org/0000-0002-1834-0498
B. Kanber https://orcid.org/0000-0003-2443-8800
F. Prados https://orcid.org/0000-0002-7872-0142
A. Saiz https://orcid.org/0000-0002-5793-8791
S. Llufriu https://orcid.org/0000-0003-4273-9121
E. Martinez-Heras https://orcid.org/0000-0001-9937-3162

REFERENCES

Andersen, K. W., Lasič, S., Lundell, H., Nilsson, M., Topgaard, D., Sellebjerg, F., Szczepankiewicz, F., Siebner, H. R., Blinkenberg, M., & Dyrby, T. B. (2020). Disentangling white-matter damage from physiological fibre orientation dispersion in multiple sclerosis. *Brain Communications*, *2*, fcaa077.

Bagnato, F., Franco, G., Li, H., Kaden, E., Ye, F., Fan, R., Chen, A., Alexander, D. C., Smith, S. A., Dortch, R., & Xu, J. (2019). Probing axons using multi-compartmental diffusion in multiple sclerosis. *Annals of Clinical Translational Neurology*, *6*, 1595–1605.

Bain, J. S., Yeatman, J. D., Schurr, R., Rokem, A., & Mezer, A. A. (2019). Evaluating arcuate fasciculus laterality measurements across dataset and tractography pipelines. *Human Brain Mapping*, *40*, 3695–3711.

Bakshi, R., Thompson, A. J., Rocca, M. A., Pelletier, D., Dousset, V., Barkhof, F., Inglese, M., Guttmann, C. R. G., Horsfield, M. A., & Filippi, M. (2008). MRI in multiple sclerosis: Current status and future prospects. *Lancet Neurology*, *7*, 615–625.

Basser, P. J., Mattiello, J., & LeBihan, D. (1994). Estimation of the effective self-diffusion tensor from the NMR spin echo. *Journal of Magnetic Resonance. Series B*, *103*, 247–254.

Basser, P. J., & Pierpaoli, C. (1996). Microstructural and physiological features of tissues elucidated by quantitative-diffusion-tensor MRI. *Journal of Magnetic Resonance. Series B*, *111*, 209–219.

Calvi, A., Carrasco, F. P., Tur, C., Chard, D. T., Stutters, J., De Angelis, F., John, N., Williams, T., Doshi, A., Samson, R. S., MacManus, D., Gandini Wheeler-Kingshott, C. A., Ciccarelli, O., Chataway, J., Barkhof, F., & MS SMART Investigators. (2022). Association of slowly expanding lesions on MRI with disability in people with secondary progressive multiple sclerosis. *Neurology*, *98*, e1783–e1793.

Coll, L., Pareto, D., Carbonell-Mirabent, P., Cobo-Calvo, Á., Arrambide, G., Vidal-Jordana, Á., Comabella, M., Castilló, J., Rodríguez-Acevedo, B., Zabalza, A., Galán, I., Midaglia, L., Nos, C., Salerno, A., Auger, C., Alberich, M., Río, J., Sastre-Garriga, J., Oliver, A., … Tur, C. (2023). Deciphering multiple sclerosis disability with deep learning attention maps on clinical MRI. *NeuroImage: Clinical*, *38*, 103376.

Estrada-López, M., Reguera-García, M. M., Pérez Rivera, F. J., & Molina, A. J. (2020). Physical disability and personality traits in multiple sclerosis. *Multiple Sclerosis and Related Disorders*, *37*, 101465.

Filippi, M., Preziosa, P., Banwell, B. L., Barkhof, F., Ciccarelli, O., De Stefano, N., Geurts, J. J. G., Paul, F., Reich, D. S., Toosy, A. T., Traboulsee, A., Wattjes, M. P., Yousry, T. A., Gass, A., Lubetzki, C., Weinshenker, B. G., & Rocca, M. A. (2019). Assessment of lesions on magnetic resonance imaging in multiple sclerosis: Practical guidelines. *Brain*, *142*, 1858–1875.

Friedman, N. P., & Robbins, T. W. (2021). The role of prefrontal cortex in cognitive control and executive function. *Neuropsychopharmacology*, *47*, 72–89.

Gabilondo, I., Martínez-Lapiscina, E. H., Martínez-Heras, E., Fraga-Pumar, E., Llufriu, S., Ortiz, S., Bullich, S., Sepulveda, M., Falcon, C., Berenguer, J., Saiz, A., Sanchez-Dalmau, B., & Villoslada, P. (2014). Trans-synaptic axonal degeneration in the visual pathway in multiple sclerosis. *Annals of Neurology*, *75*, 98–107.

Greve, D. N., & Fischl, B. (2009). Accurate and robust brain image alignment using boundary-based registration. *NeuroImage*, *48*, 63–72.

Jeurissen, B., Tournier, J.-D., Dhollander, T., Connelly, A., & Sijbers, J. (2014). Multi-tissue constrained spherical deconvolution for improved analysis of multi-shell diffusion MRI data. *NeuroImage*, *103*, 411–426.

Kaden, E., Kelm, N. D., Carson, R. P., Does, M. D., & Alexander, D. C. (2016). Multi-compartment microscopic diffusion imaging. *NeuroImage*, *139*, 346–359.

Klein, A., Ghosh, S. S., Bao, F. S., Giard, J., Häme, Y., Stavsky, E., Lee, N., Rossa, B., Reuter, M., Chaibub Neto, E., & Keshavan, A. (2017). Mindboggling morphometry of human brains. *PLoS Computational Biology*, *13*, e1005350.

Kurtzke, J. F. (1983). Rating neurologic impairment in multiple sclerosis: An Expanded Disability Status Scale (EDSS). *Neurology*, *33*, 1444–1452.

Landman, B. A., Wan, H., Bogovic, J. A., Bazin, P.-L., & Prince, J. L. (2010). Resolution of crossing fibers with constrained compressed sensing using traditional diffusion tensor MRI. *Proceedings of SPIE the International Society for Optical Engineering*, *7623*, 76231H.

Lassmann, H., Brück, W., & Lucchinetti, C. F. (2007). The immunopathology of multiple sclerosis: An overview. *Brain Pathology*, *17*, 210–218.

Lipp, I., Parker, G. D., Tallantyre, E. C., Goodall, A., Grama, S., Patitucci, E., Heveron, P., Tomassini, V., & Jones, D. K. (2020). Tractography in the presence of multiple sclerosis lesions. *NeuroImage*, *209*, 116471.

Llufriu, S., Blanco, Y., Martinez-Heras, E., Casanova-Molla, J., Gabilondo, I., Sepulveda, M., Falcon, C., Berenguer, J., Bargallo, N., Villoslada, P., Graus, F., Valls-Sole, J., & Saiz, A. (2012). Influence of corpus callosum damage on cognition and physical disability in multiple sclerosis: A multimodal study. *PLoS One*, *7*, e37167.

Llufriu, S., Martinez-Heras, E., Solana, E., Sola-Valls, N., Sepulveda, M., Blanco, Y., Martinez-Lapiscina, E. H., Andorra, M., Villoslada, P., Prats-Galino, A., & Saiz, A. (2017). Structural networks involved in attention and executive functions in multiple sclerosis. *NeuroImage: Clinical*, *13*, 288–296.

Lublin, F. D., Reingold, S. C., Cohen, J. A., Cutter, G. R., Sørensen, P. S., Thompson, A. J., Wolinsky, J. S., Balcer, L. J., Banwell, B., Barkhof, F., Bebo, B., Jr., Calabresi, P. A., Clanet, M., Comi, G., Fox, R. J., Freedman, M. S., Goodman, A. D., Inglese, M., Kappos, L., … Polman, C. H. (2014). Defining the clinical course of multiple sclerosis: The 2013 revisions. *Neurology*, *83*, 278–286.

Martinez-Heras, E., Grussu, F., Prados, F., Solana, E., & Llufriu, S. (2021). Diffusion-weighted imaging: Recent advances and applications. *Seminars in Ultrasound, CT, and MR*, *42*, 490–506.

Martínez-Heras, E., Solana, E., Prados, F., Andorrà, M., Solanes, A., López-Soley, E., Montejo, C., Pulido-Valdeolivas, I., Alba-Arbalat, S., Sola-Valls, N., Sepúlveda, M., Blanco, Y., Saiz, A., Radua, J., & Llufriu, S. (2020). Characterization of multiple sclerosis lesions with distinct clinical correlates through quantitative diffusion MRI. *NeuroImage: Clinical*, *28*, 102411.

Martinez-Heras, E., Solana, E., Vivó, F., Lopez-Soley, E., Calvi, A., Alba-Arbalat, S., Schoonheim, M. M., Strijbis, E. M., Vrenken, H., Barkhof, F., Rocca, M. A., Filippi, M., Pagani, E., Groppa, S., Fleischer, V., Dineen, R. A., Bellenberg, B., Lukas, C., Pareto, D., … Llufriu, S. (2023). Diffusion-based structural connectivity patterns of multiple sclerosis phenotypes. *Journal of Neurology, Neurosurgery, and Psychiatry*, *94*, 916–923.

Martínez-Heras, E., Varriano, F., Prčkovska, V., Laredo, C., Andorrà, M., Martínez-Lapiscina, E. H., Calvo, A., Lampert, E., Villoslada, P., Saiz, A., Prats-Galino, A., & Llufriu, S. (2015). Improved framework for tractography reconstruction of the optic radiation. *PLoS One*, *10*, e0137064.

Meijer, K. A., Steenwijk, M. D., Douw, L., Schoonheim, M. M., & Geurts, J. J. G. (2020). Long-range connections are more severely damaged and relevant for cognition in multiple sclerosis. *Brain*, *143*, 150–160.

Parmenter, B. A., Weinstock-Guttman, B., Garg, N., Munschauer, F., & Benedict, R. H. B. (2007). Screening for cognitive impairment in multiple sclerosis using the symbol digit modalities test. *Multiple Sclerosis*, *13*, 52–57.

Patenaude, B., Smith, S. M., Kennedy, D. N., & Jenkinson, M. (2011). A Bayesian model of shape and appearance for subcortical brain segmentation. *NeuroImage*, *56*, 907–922.

Reid, L. B., Sale, M. V., Cunnington, R., Mattingley, J. B., & Rose, S. E. (2017). Brain changes following four weeks of unimanual motor training: Evidence from fMRI-guided diffusion MRI tractography. *Human Brain Mapping*, *38*, 4302–4312.

Sbardella, E., Tona, F., Petsas, N., & Pantano, P. (2013). DTI measurements in multiple sclerosis: Evaluation of brain damage and clinical implications. *Multiple Sclerosis International*, *2013*, 671730.

Sepulcre, J., Masdeu, J. C., Goñi, J., Arrondo, G., Vélez de Mendizábal, N., Bejarano, B., & Villoslada, P. (2009). Fatigue in multiple sclerosis is associated with the disruption of frontal and parietal pathways. *Multiple Sclerosis*, *15*, 337–344.

Shine, J. M., Lewis, L. D., Garrett, D. D., & Hwang, K. (2023). The impact of the human thalamus on brain-wide information processing. *Nature Reviews. Neuroscience*, *24*, 416–430.

Smith, R. E., Tournier, J.-D., Calamante, F., & Connelly, A. (2012). Anatomically-constrained tractography: Improved diffusion MRI streamlines tractography through effective use of anatomical information. *NeuroImage*, *62*, 1924–1938.

Solana, E., Martinez-Heras, E., Casas-Roma, J., Calvet, L., Lopez-Soley, E., Sepulveda, M., Sola-Valls, N., Montejo, C., Blanco, Y., Pulido-Valdeolivas, I., Andorra, M., Saiz, A., Prados, F., & Llufriu, S. (2019). Modified connectivity of vulnerable brain nodes in multiple sclerosis, their impact on cognition and their discriminative value. *Scientific Reports*, *9*, 20172.

Solana, E., Martinez-Heras, E., Martinez-Lapiscina, E. H., Sepulveda, M., Sola-Valls, N., Bargalló, N., Berenguer, J., Blanco, Y., Andorra, M., Pulido-Valdeolivas, I., Zubizarreta, I., Saiz, A., & Llufriu, S. (2018). Magnetic resonance markers of tissue damage related to connectivity disruption in multiple sclerosis. *NeuroImage: Clinical*, *20*, 161–168.

Strober, L. B., Bruce, J. M., Arnett, P. A., Alschuler, K. N., Lebkuecher, A., Di Benedetto, M., Cozart, J., Thelen, J., Guty, E., & Roman, C. (2020). A

new look at an old test: Normative data of the symbol digit modalities test-oral version. *Multiple Sclerosis and Related Disorders*, *43*, 102154.

Sumowski, J. F., Benedict, R., Enzinger, C., Filippi, M., Geurts, J. J., Hamalainen, P., Hulst, H., Inglese, M., Leavitt, V. M., Rocca, M. A., Rosti-Otajarvi, E. M., & Rao, S. (2018). Cognition in multiple sclerosis: State of the field and priorities for the future. *Neurology*, *90*, 278–288.

Thompson, A. J., Banwell, B. L., Barkhof, F., Carroll, W. M., Coetzee, T., Comi, G., Correale, J., Fazekas, F., Filippi, M., Freedman, M. S., Fujihara, K., Galetta, S. L., Hartung, H. P., Kappos, L., Lublin, F. D., Marrie, R. A., Miller, A. E., Miller, D. H., Montalban, X., … Cohen, J. A. (2018). Diagnosis of multiple sclerosis: 2017 revisions of the McDonald criteria. *Lancet Neurology*, *17*, 162–173.

Tournier, J.-D., Smith, R., Raffelt, D., Tabbara, R., Dhollander, T., Pietsch, M., Christiaens, D., Jeurissen, B., Yeh, C.-H., & Connelly, A. (2019). MRtrix3: A fast, flexible and open software framework for medical image processing and visualisation. *NeuroImage*, *202*, 116137.

Wasserthal, J., Neher, P., & Maier-Hein, K. H. (2018). TractSeg—Fast and accurate white matter tract segmentation. *NeuroImage*, *183*, 239–253.

Wiegell, M. R., Larsson, H. B., & Wedeen, V. J. (2000). Fiber crossing in human brain depicted with diffusion tensor MR imaging. *Radiology*, *217*, 897–903.

Yeatman, J. D., Dougherty, R. F., Myall, N. J., Wandell, B. A., & Feldman, H. M. (2012). Tract profiles of white matter properties: Automating fiber-tract quantification. *PLoS One*, *7*, e49790.

Zhang, J., Cortese, R., De Stefano, N., & Giorgio, A. (2021). Structural and functional connectivity substrates of cognitive impairment in multiple sclerosis. *Frontiers in Neurology*, *12*, 671894.

How to cite this article: Vivó, F., Solana, E., Calvi, A., Lopez-Soley, E., Reid, L. B., Pascual-Diaz, S., Garrido, C., Planas-Tardido, L., Cabrera-Maqueda, J. M., Alba-Arbalat, S., Sepulveda, M., Blanco, Y., Kanber, B., Prados, F., Saiz, A., Llufriu, S., & Martinez-Heras, E. (2024). Microscopic fractional anisotropy outperforms multiple sclerosis lesion assessment and clinical outcome associations over standard fractional anisotropy tensor. *Human Brain Mapping*, *45*(8), e26706. https://doi.org/10.1002/hbm.26706